

# Polarization-Locked Floquet Higher-Order Topological Insulators in Synthetic Dimension

Zhuoxiong Liu, Weiwei Liu,\* Lingzhi Zheng, Shuaifei Ren, Xiaolong Su, Yufan Ding, Bing Wang,\* and Peixiang Lu\*

Floquet engineering provides a powerful tool for exploring topological physics. Systems incorporating Floquet driving can exhibit intriguing topological phenomena without correspondence with static counterparts. Recently, following the development of higher-order topology, Floquet higher-order topological insulators have drawn great attention since its peculiarity in the band structure and topological states. Here the higher-order topological insulator is theoretically demonstrated via Floquet engineering in synthetic frequency dimension. To this end, a 1D Floquet topological insulator is first constructed by introducing periodic driving to the frequency lattice, and the corresponding 0 and  $\pi$  edge states are demonstrated. On this basis, a Floquet higher-order topological insulator supporting 0 and  $\pi$  corner states is realized by stacking the chains of the 1D Floquet topological insulators with dimerized couplings. Particularly, it is found that the distributions of 0 and  $\pi$  modes occupy the frequency lattices with orthogonal polarizations, which indicate polarization-locked topological states and enable selective excitation of the topological edge/corner states with specific polarizations. This work lays the foundation for realizing controllable Floquet systems and opens an avenue for exploring higher-order topological physics with synthetic dimension, which shows great promise for applications in polarization conversion and quantum information processing.

nontrivial higher-order bulk topology.<sup>[5]</sup> Recently, following the development of higher-order topological insulators, Floquet higher-order topological insulators (FHOTIs) gradually came into the views of people.<sup>[6–15]</sup> The core concept of FHOTIs is “Floquet engineering,” which enables FHOTIs to possess many intriguing phenomena, such as anomalous Floquet  $\pi$  corner modes<sup>[6,7,9]</sup> and oscillated corner state.<sup>[16]</sup> In photonics, previous works concerning higher-order topology in Floquet systems mainly focus on the real-space physical structures.<sup>[11]</sup> However, the Floquet systems generally possess various topological phases demanding different physical parameters and structures. To access different topological phases, the refabrication of the physical structures is necessitated, which increases the difficulty of experiments and hinders their feasibility in applications.

The recently proposed synthetic dimensions provide a powerful approach to realize controllable Floquet systems since the flexibility and programmability in manipulating system parameters.<sup>[17–31]</sup>

Synthetic dimensions are used to mimic the dynamics in real space, where the high-dimensional physical phenomena could be simulated with fewer geometric dimensions.<sup>[17,18,30]</sup> In photonics, synthetic dimensions are formed by utilizing external degrees of freedom of photonics such as frequency,<sup>[32–39]</sup> orbital angular momentum,<sup>[40–46]</sup> transverse spatial super-modes,<sup>[47,48]</sup> and time of arrival light pulses.<sup>[49–52]</sup> Among these approaches, the synthetic frequency dimension has become a versatile platform for exploring topological physics since its feasibility and flexibility in realizing artificial gauge potential.<sup>[53,54]</sup> Numerous topological phenomena have been demonstrated in synthetic frequency dimension, such as 3D topological insulators,<sup>[55]</sup> photonic Weyl semimetals,<sup>[32]</sup> non-Hermitian topological bands braiding,<sup>[36]</sup> topological spin pump,<sup>[56]</sup> and higher-order topological insulators.<sup>[34]</sup> The versatility of synthetic frequency dimensions not only enriches the understanding of topological physics but also opens new avenues for designing advanced photonic devices with tailored functionalities and unprecedented capabilities.

In this work, we construct FHOTIs in the synthetic frequency dimension. We first illustrate the theoretical model of 1D

## 1. Introduction

Higher-order topological insulators represent a recently discovered class of topological phase, which shows that not only edge and surface states but also states localized to corners can possess robust properties.<sup>[1–4]</sup> For example, a 2D second-order topological insulator can host 0D corner states protected by

Z. Liu, W. Liu, L. Zheng, S. Ren, X. Su, Y. Ding, B. Wang, P. Lu  
Wuhan National Laboratory for Optoelectronics and School of Physics  
Huazhong University of Science and Technology  
Wuhan, Hubei 430074, China  
E-mail: [lwust@hust.edu.cn](mailto:lwust@hust.edu.cn); [wangbing@hust.edu.cn](mailto:wangbing@hust.edu.cn);  
[lupeixiang@hust.edu.cn](mailto:lupeixiang@hust.edu.cn)

P. Lu  
Hubei Key Laboratory of Optical Information and Pattern Recognition  
Wuhan Institute of Technology  
Wuhan, Hubei 430205, China

 The ORCID identification number(s) for the author(s) of this article can be found under <https://doi.org/10.1002/lpor.202401156>

DOI: 10.1002/lpor.202401156

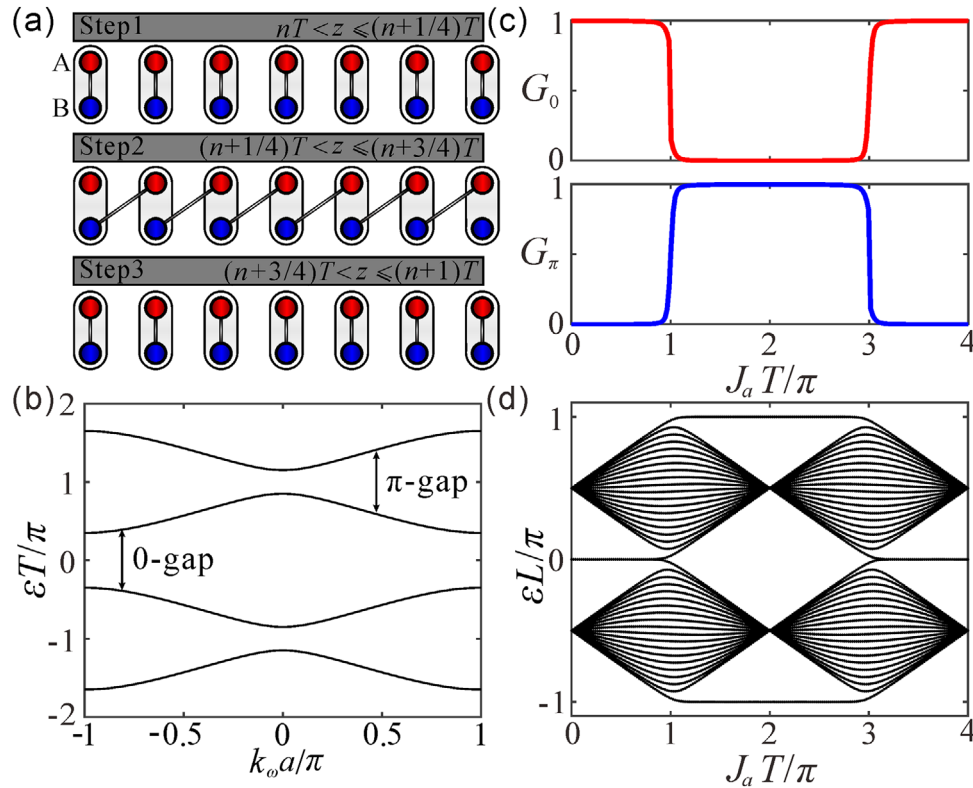


**Figure 1.** a) Driving protocol of three-step model in a 1D lattice. During the steps 1 and 3, the intercell coupling is zero and hopping occurs within the unit cell. In step 2, the intercell coupling is activated and intracell coupling is zero. The evolution length of steps 1 and 3 is  $L/4$  and the evolution length of step 2 is  $L/2$ . b) The Floquet band structure of 1D FTI, with the occurrence of 0 and  $\pi$  gap. c) The topological invariants  $G_0$  and  $G_\pi$  as the function of  $J_a$  with  $J_b = \pi / L$ , manifest the processes of topological phase transition. d) The Floquet quasi-energy is the function of  $J_a$  with  $J_b = \pi / L$ , which clearly features 0 and  $\pi$  edge states.

Floquet topological insulator (FTI) and its photonic implementation, which utilizes the synthetic frequency dimension in a dynamically modulated waveguide. The employed synthetic lattices are created through polarization inter-band transition, which introduces additional polarization freedom and presents a significant distinction from those utilizing photonic intra-band transitions.<sup>[57,58]</sup> Based on this, we construct the FHOTIs in a 1D periodically modulated waveguide array and demonstrate the topological 0 and  $\pi$  modes. Interestingly, we find that the distributions of 0 and  $\pi$  modes occupy the frequency lattices with orthogonal polarizations, which indicate polarization-locked topological states and enable selective excitation of the topological edge/corner states with specific polarizations.

## 2. Results and Discussion

### 2.1. Theoretical Model of 1D Floquet Topological Insulator

We start from the theoretical model of our 1D FTI, which serves as the basic building blocks for constructing FHOTIs. As shown in **Figure 1a**, we consider a 1D discrete lattice with two site species A and B (marked by red and blue sites). To get the desired topological phases, the couplings in the lattice are subjected to a time-dependent modulation scheme, where a full driving cycle comprises a sequence of three individual steps. These steps are di-

vided into two types of operation: steps 1 and 3 realize the hopping within the unit cell, whereas the coupling between the unit cell is accomplished in step 2. The evolution length of steps 1, 2, and 3 is  $T/4$ ,  $T/2$ , and  $T/4$  respectively ( $T$  is the driving period). This arrangement is vital for realizing chirality in our model (see Section S1, Supporting Information). The associated Bloch Hamiltonian  $H(k, t)$  is therefore time-periodic,  $H(k, t) = H(k, t + T)$ , which is given by

$$H(k, t) = \begin{cases} H_a(k), & jT \leq t < (j+1/4)T, \\ H_b(k), & (j+1/4)T \leq t < (j+3/4)T, \\ H_a(k), & (j+3/4)T \leq t < (j+1)T \end{cases} \quad (1)$$

where  $H_a(k) = J_a \sigma_x$  and  $H_b(k) = J_b \cos(k_0 a) \sigma_x + J_b \sin(k_0 a) \sigma_y$ , with  $\sigma_x$  and  $\sigma_y$  being Pauli matrix.  $J_a$  ( $J_b$ ) represents the strength of intracell (intercell) coupling and  $a$  is the lattice constant.  $H(k, t)$  possesses chiral symmetry with  $\Gamma H(k, t) \Gamma = -H(k, -t)$ , where  $\Gamma$  is the chirality operator. Due to periodicity in  $t$ , the Floquet theory can be applied to derive a band structure of so-called quasi-energy, the corresponding band structure of our model under periodic boundary conditions is presented in **Figure 1b**. The Floquet spectrum is periodic in its quasi-energies, in full correspondence to the periodicity in the transverse momentum caused by Bloch's theorem. Consequently, the 0 and  $\pi$  gap can be defined

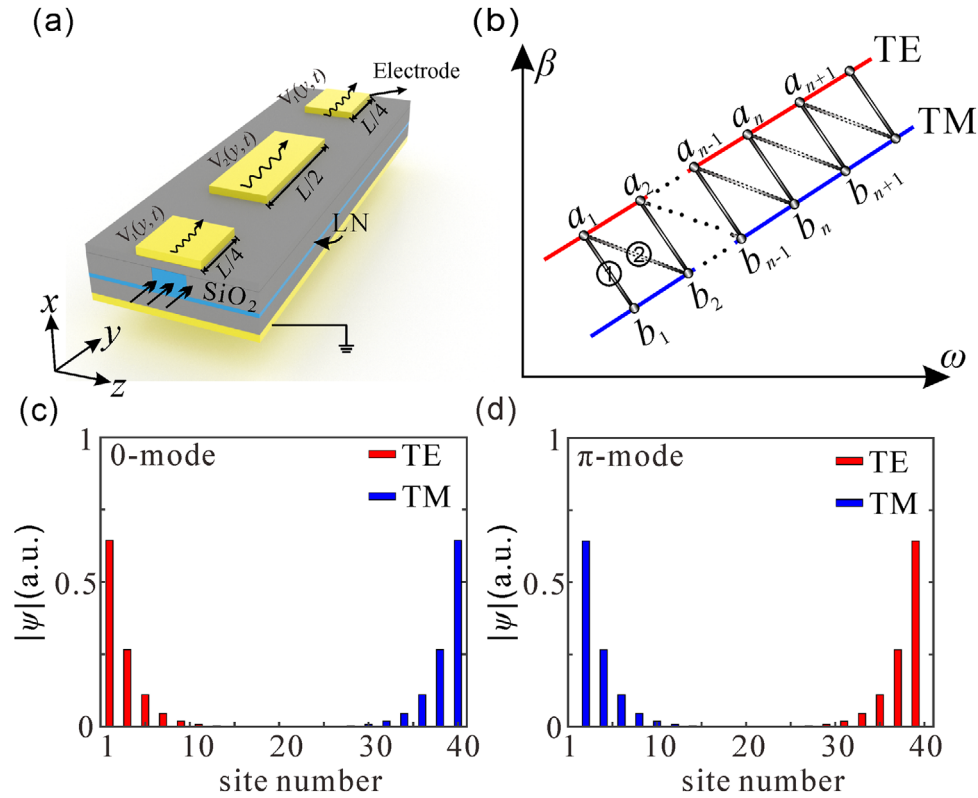


**Figure 2.** a) The diagram of a photonic waveguide undergoing periodic modulation, which is realized by periodically cascading the electrodes along the propagating directions. b) Polarization inter-band transition between TE and TM modes. c) The distributions of 0 edge state, which has components only on TE (TM) polarization at left (right) edges. d) The distributions of  $\pi$  edge state, with components only on TM (TE) polarization at left (right) edges.

in our model due to the periodicity of the quasi-energy, as shown in Figure 1b.

To characterize the topology of this model, a  $\mathbb{Z}$ -valued invariant can be defined for the quasi-energy gap at 0 or  $\pi$ . This  $\mathbb{Z}$ -valued invariant is used to define the topology of 1D periodically driven system with chiral symmetry, which is also appropriate to our model.<sup>[59,60]</sup> To calculate this invariant, we first resort to

the time-evolution operator, given by  $U(k, t) = P e^{-i \int_0^t H(k, \tau) d\tau}$  ( $P$  is the time-ordering operator). Then we can get a time-independent effective Hamiltonian  $H_{\text{eff}}(k) = (i/T) \ln U(k, T)$ , describing the effective stroboscopic dynamics after multiples of the period. A periodized evolution operator  $V_\epsilon(k, t)$  combining the effect of  $U(k, t)$  and  $H_{\text{eff}}(k)$  could be then defined, which is expressed as

$$V_\epsilon(k, t) = U(k, t) e^{i H_{\text{eff}}^\epsilon(k) t} \quad (2)$$

where the subscript  $\epsilon = 0, \pi$  is employed to indicate the gap of the band structure. It could be found that both 0 and  $\pi$  gaps could exist in our model, the corresponding topological invariant is calculated by

$$G_\epsilon = \frac{i}{2\pi} \int_{\text{BZ}} \text{tr}((V_\epsilon^+)^{-1} \frac{\partial}{\partial k} V_\epsilon^+) dk \quad (3)$$

where  $V_\epsilon + \epsilon$  is obtained from the periodized evolution operator at half period. The numerical results of  $G_0$  and  $G_\pi$  as a function of  $J_a$  is presented in Figure 1c, where the intercell coupling  $J_b$  is fixed to  $\pi/T$ . When  $0 < J_a < \pi/T$ ,  $G_0 = 1$ ,  $G_\pi = 0$ , whereas  $G_0 = 0$ ,  $G_\pi = 1$  while  $\pi/T < J_a < 3\pi/T$  (full phase diagram is displayed in the Section S1, Supporting Information). A non-zero  $G_0$  ( $G_\pi$ ) indicates a topologically nontrivial phase and through bulk-edge correspondence, it corresponds to the edge 0 ( $\pi$ ) modes within the 0 ( $\pi$ ) gap, as verified by the open boundary quasi-energy spectrum in Figure 1d.

## 2.2. Photonic Implementation of 1D Floquet Topological Insulator

The photonic realization of this 1D FTI requires a high degree of control over the couplings presented in the lattice. Synthetic frequency dimension provides a convenient approach to manipulating the coupling between individual sites, thus showing great promise for constructing photonic topological insulators. Figure 2a displays our scheme for realizing the 1D FTI utilizing synthetic frequency dimension. Consider a photonic waveguide undergoing travelling wave modulation  $V(y, t) = V_1(y) \cos(\Omega_1 t - q_1 y) + V_2(y) \cos(\Omega_2 t - q_2 y)$ , where  $V_1(y)$  and  $V_2(y)$  are amplitude of modulations with frequencies and wavevectors being  $\Omega_1, \Omega_2$  and  $q_1, q_2$  respectively. The waveguide is assumed to support a pair of transverse-electric-like (TE) and transverse-magnetic-like (TM)

modes. The travelling wave modulation would cause an optical permittivity perturbation  $\Delta\epsilon(\gamma, t) = \Delta\epsilon_1(\gamma, t) + \Delta\epsilon_2(\gamma, t)$ , which induces the polarization inter-band transitions between TE and TM modes.<sup>[61–64]</sup> The corresponding coupled-mode equation is given by (see Section S2, Supporting Information)

$$\begin{aligned} i\frac{\partial a_n}{\partial \gamma} &= J_1(\gamma)b_n + J_2(\gamma)b_{n-1}, \\ i\frac{\partial b_n}{\partial \gamma} &= J_1(\gamma)a_n + J_2(\gamma)a_{n+1} \end{aligned} \quad (4)$$

where  $a_n$  and  $b_n$  represent the complex amplitudes of TE and TM modes. Here  $\gamma$  plays the role of “time” as in the Schrodinger equation. Equation (4) describes a 1D lattice with sites represented by TE and TM modes with different frequencies alternatively, as shown in Figure 2b. The structure of this synthetic lattice can be actually modeled as that in Figure 1a, where a pair of TE and TM modes constitute two site species A and B. With this framework,  $J_1(\gamma)$  and  $J_2(\gamma)$  represent intracell and intercell couplings respectively, with  $J_1(\gamma) = i\epsilon_0\omega_n \iint e^* \Delta\epsilon_1(\gamma)e_2 dx dy / 2$ ,  $J_2(\gamma) = i\epsilon_0\omega_n \iint e^* \Delta\epsilon_2(\gamma)e_2 dx dy / 2$ .

As mentioned above, to realize FTI in the synthetic lattice, the couplings between lattice sites need to be subjected to time-dependent modulations comprising three individual steps in a driving cycle. To this end, we cascade three modulators within one period, the length of which are  $L/4$ ,  $L/2$ , and  $L/4$  respectively ( $L$  represents the periodicity), as shown in Figure 2a. The form of travelling wave modulations in three modulators are set as

$$\begin{aligned} V_1(\gamma) &= V_a, V_2(\gamma) = 0, jL \leq \gamma < (j+1/4)L, \\ V_1(\gamma) &= 0, V_2(\gamma) = V_b, (j+1/4)L \leq \gamma < (j+3/4)L, j \in \mathbb{Z}, \\ V_1(\gamma) &= V_a, V_2(\gamma) = 0, (j+3/4)L \leq \gamma < (j+1)L \end{aligned} \quad (5)$$

Under this arrangement,  $V_2(\gamma)$  is 0 within the first and third modulators so that the intercell couplings  $J_2(\gamma)$  is zero, and the associated coupling occurs within the unit cell, i.e.,  $TE_n$  to  $TM_n$ . In contrast,  $V_1(\gamma)$  is 0 in the second modulator and the coupling only exists between the unit cell, i.e.,  $TE_n$  to  $TM_{n+1}$ . The corresponding Hamiltonian governing the system is  $\gamma$ -periodic, which is given by

$$H(\gamma) = \sum_n J_1(\gamma)a_n^+ b_n + J_2(\gamma)a_n^+ b_{n-1} + h.c. \quad (6)$$

with  $J_1(\gamma)$  and  $J_2(\gamma)$  expressed as

$$\begin{aligned} J_1(\gamma) &= J_a, J_2(\gamma) = 0, jL \leq \gamma < (j+1/4)L, \\ J_1(\gamma) &= 0, J_2(\gamma) = J_b, (j+1/4)L \leq \gamma < (j+3/4)L, j \in \mathbb{Z}, \\ J_1(\gamma) &= J_a, J_2(\gamma) = 0, (j+3/4)L \leq \gamma < (j+1)L \end{aligned} \quad (7)$$

where  $a_n$  ( $b_n$ ) are annihilation operators of TE (TM) mode. As confirmed in Section 2.1, this model would manifest non-trivial topology under an appropriate combination of  $J_a$  and  $J_b$ .

To characterize the topology of this model, we truncate the synthetic lattice at  $n = \pm 20$  and calculate the corresponding edge states. The synthetic frequency lattice could be truncated by adding artificial boundary, which is realized by carefully engineering the dispersion curve of waveguide.<sup>[53]</sup> Figure 2c,d plots the distribution of 0 and  $\pi$  edge states with  $J_a = 0.5\pi/L$ ,  $J_b = \pi/L$  and  $J_a = 1.5\pi/L$ ,  $J_b = \pi/L$  respectively, both of which mainly localize at boundaries of the lattice and decay rapidly into the

bulk. Importantly, the distributions of 0 and  $\pi$  states occupy the frequency lattices with orthogonal polarization, indicating polarization-locked topological states. This locking mechanism is closely related to the chirality of the Hamiltonian (see Section S3, Supporting Information). For example, as shown in Figure 2c,d, the 0 state is distributed on the odd sites of the lattice while the  $\pi$ -energy state is distributed on the even sites on left half side of the lattice. Since the peculiar lattice structure where the odd (even) sites are consisted of TE(TM) modes, the 0-energy state possesses the TE polarization, while the  $\pi$ -energy state possesses the TM polarization. On the right half side, the polarization of the 0-energy and  $\pi$ -energy states exchanges due to the inversion symmetry of the lattice.

### 2.3. 2D Floquet Higher-Order Topological Insulators and Polarization-Locked Corner States

The 1D FTI in synthetic frequency dimension provides an excellent building block for constructing FHOTIs. As shown in Figure 3a, the system consists of 1D dynamically modulated waveguide arrays, where the individual waveguides are coupled together by evanescent waves. Therefore, the modes in the individual waveguide would undergo polarization inter-band transitions, thus forming a synthetic frequency lattice. As shown in previous section, the synthetic frequency lattice can form 1D FTI under Floquet driving. The couplings between waveguides play the role of stacking the 1D FTI along  $z$  axis, resulting in a 2D frequency lattice in synthetic  $\omega$ - $z$  space, as shown in Figure 3b. The structure of this synthetic lattice is similar with the 2D Su-Schrieffer-Heeger model, except that the couplings along  $\omega$ -direction are subjected to time-dependent modulation (see Section S4, Supporting Information). The Hamiltonian governing the dynamics of this lattice is still periodic under Floquet driving, i.e.,  $H(\gamma + L) = H(\gamma)$ , which is given by

$$\begin{aligned} H(\gamma) &= \sum_{m,n} J_{s1} b_{m,n}^+ a_{m,n} + J_{s1} c_{m,n}^+ d_{m,n} + J_{s2} b_{m,n}^+ a_{m+1,n} + J_{s2} c_{m,n}^+ d_{m+1,n} \\ &+ h.c. + \sum_{m,n} J_{\omega 1}(\gamma) a_{m,n}^+ d_{m,n} + J_{\omega 1}(\gamma) b_{m,n}^+ c_{m,n} \\ &+ J_{\omega 2}(\gamma) d_{m,n}^+ a_{m,n+1} + J_{\omega 2}(\gamma) c_{m,n}^+ b_{m,n+1} h.c. \end{aligned} \quad (8)$$

where  $a_{m,n}$ ,  $b_{m,n}$ ,  $c_{m,n}$ ,  $d_{m,n}$  represent annihilators in a unit cell with  $m, n$  representing the unit cell index of  $z$  and  $\omega$  axes.  $J_{s1}$  and  $J_{s2}$  are dimerized couplings along  $z$ -direction.  $J_{\omega 1}(\gamma)$  and  $J_{\omega 2}(\gamma)$  represent the couplings of frequency dimension, which satisfy

$$\begin{aligned} J_{\omega 1}(\gamma) &= J_a, J_{\omega 2}(\gamma) = 0, jL \leq \gamma < (j+1/4)L, \\ J_{\omega 1}(\gamma) &= 0, J_{\omega 2}(\gamma) = J_b, (j+1/4)L \leq \gamma < (j+3/4)L, j \in \mathbb{Z}, \\ J_{\omega 1}(\gamma) &= J_a, J_{\omega 2}(\gamma) = 0, (j+3/4)L \leq \gamma < (j+1)L \end{aligned} \quad (9)$$

Therefore, the Floquet operator is given by

$$U = e^{-iH_1 L/4} e^{-iH_2 L/4} e^{-iH_1 L/4} \quad (10)$$

where  $H_1$  and  $H_2$  are equal to  $H(\gamma)$  in the range of  $jL \leq \gamma < (j+1/4)L$  and  $(j+1/4)L \leq \gamma < (j+3/4)L$  respectively.

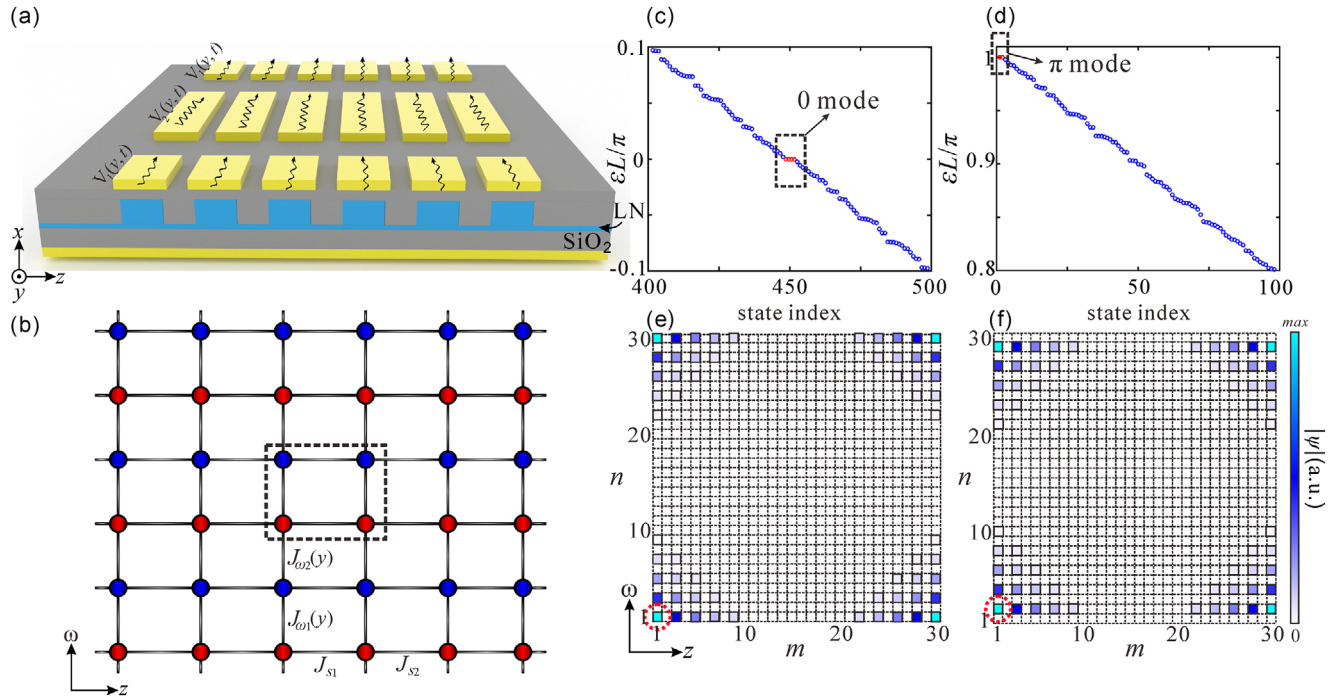


**Figure 3.** a) The diagram of waveguide array undergoing traveling-wave modulation. b) The equivalent synthetic lattice model with two orthogonal directions  $\omega$  and  $z$ , the unit cell of which consists of four lattice sites inside the dashed box. c) Quasi-energy distribution of the lattice with 0 corner modes. The coupling constants along  $z$  and  $\omega$  axes are set as  $J_{s1} = 0.5\pi/L$ ,  $J_{s2} = \pi/L$  and  $J_a = 0.5\pi/L$ ,  $J_b = \pi/L$ . d) Quasi-energy distribution of the lattice with  $J_a = 1.5\pi/L$ . The model supports  $\pi$  corner modes in this scene. e, f) State distribution of 0 and  $\pi$  corner modes, which localize at the corner and decay rapidly into the bulk.

The model proposed above manifests non-trivial topology with the existence of 0 corner modes and  $\pi$  corner modes under appropriate coupling strength. To see this more clearly, we diagonalize the Floquet operator  $U$  to get the quasi-energy  $\epsilon$  and the corresponding eigenstates under open boundary condition in both directions. Figure 3c displays the full quasi-energy distribution of the lattice with  $J_{s1} = 0.5\pi/L$ ,  $J_{s2} = \pi/L$  and  $J_a = 0.5\pi/L$ ,  $J_b = \pi/L$ , which features the 0 corner modes in the 0-energy gap. Figure 3d plots the quasi-energy distribution as  $J_a$  is changed to  $1.5\pi/L$ , in which the lattice supports  $\pi$  corner modes. Figure 3e, f demonstrates the state distributions of 0 and  $\pi$  modes, which localize at the corner of the lattice and decay rapidly into the bulk. As mentioned above, while the synthetic 1D FTIs are in the phase of topological non-trivial, the 0 or  $\pi$  edge states would appear. Then a chain of 1D topological insulators would be coupled together with dimerized strength. In the fully dimerized scene with  $J_{s1} = 0$ ,  $J_{s2} \neq 0$ , the 0 or  $\pi$  edge states at the first (last) chain would be decoupled from others, thus forming the 0 or  $\pi$  corner states. While  $J_{s1} \neq 0$ , the model could support corner states in the range of  $J_{s1} < J_{s2}$ <sup>[65]</sup> ( $J_a$  and  $J_b$  should satisfy that the 1D topological insulators are in the phase of topological non-trivial).

As shown in Figure 3e, f, the distributions of 0 and  $\pi$  corner modes also occupy the frequency lattices with orthogonal polarization, and such characteristics enable to realize the polarization-locked 0 and  $\pi$  corner modes (see Section S3, Supporting Information). To illustrate this, the state evolutions of the lattice governed by the Floquet Hamiltonian  $H(\gamma)$  under open boundary condition is calculated. The lattice size is set as  $30 \times 30$  with  $J_{s1} = 0.5\pi/L$ ,  $J_{s2} = \pi/L$ . In Figure 4a, the coupling strengths

are set as  $J_a = 0.5\pi/L$ ,  $J_b = \pi/L$ , where the lattice supports 0-corner mode with TE polarization at the bottom-left corner. The excited site is located at  $m = 1$ ,  $n = 1$ , which corresponds to the waveguide modes input from the first waveguide with TE polarization ( $\omega = \omega_0 + \Omega_1$ ). As shown in Figure 4b, c, the 0-corner modes are excited and it can be localized at the bottom-left ( $m = 1$ ,  $n = 1$ ) corner throughout the propagation. For comparison, the TM modes are injected instead in Figure 4d. The excited modes delocalize and diffuse into the bulk gradually in the propagation process, which demonstrates the polarization-locked characteristic. Similar results could also be observed in  $\pi$  corner modes. In this situation,  $J_a$  is changed to  $1.5\pi/L$  so that the lattice will support the  $\pi$  corner modes. The TM mode is injected with frequency  $\omega = \omega_0 + \Omega_1 + \Omega_2$ , corresponding to the excitation at  $m = 1$ ,  $n = 2$  on the synthetic lattice, as shown in Figure 4e. The  $\pi$  corner modes can be localized at the initial excitation spot throughout the propagation. For comparison, as the input mode is changed to TE polarization with frequency  $\omega = \omega_0 + \Omega_1$ , the  $\pi$  modes cannot be excited so that the mode would diffuse into the bulk in the processes of evolution, as displayed in Figure 4h.

In the end, we provide some discussions about the experimental implementation of the proposal for realizing polarization-locked FHOTIs in synthetic frequency lattice. As analyzed above, the polarization inter-band transitions are induced by the off-diagonal modulations to the relative permittivity, which can be achieved with electro-optic LiNbO<sub>3</sub> waveguides. For example, in an X-cut, Y-propagating LiNbO<sub>3</sub> waveguide undergoing traveling-wave modulations, the electro-optical tensor element  $r_{51}$  is utilized when the external microwave electric field is

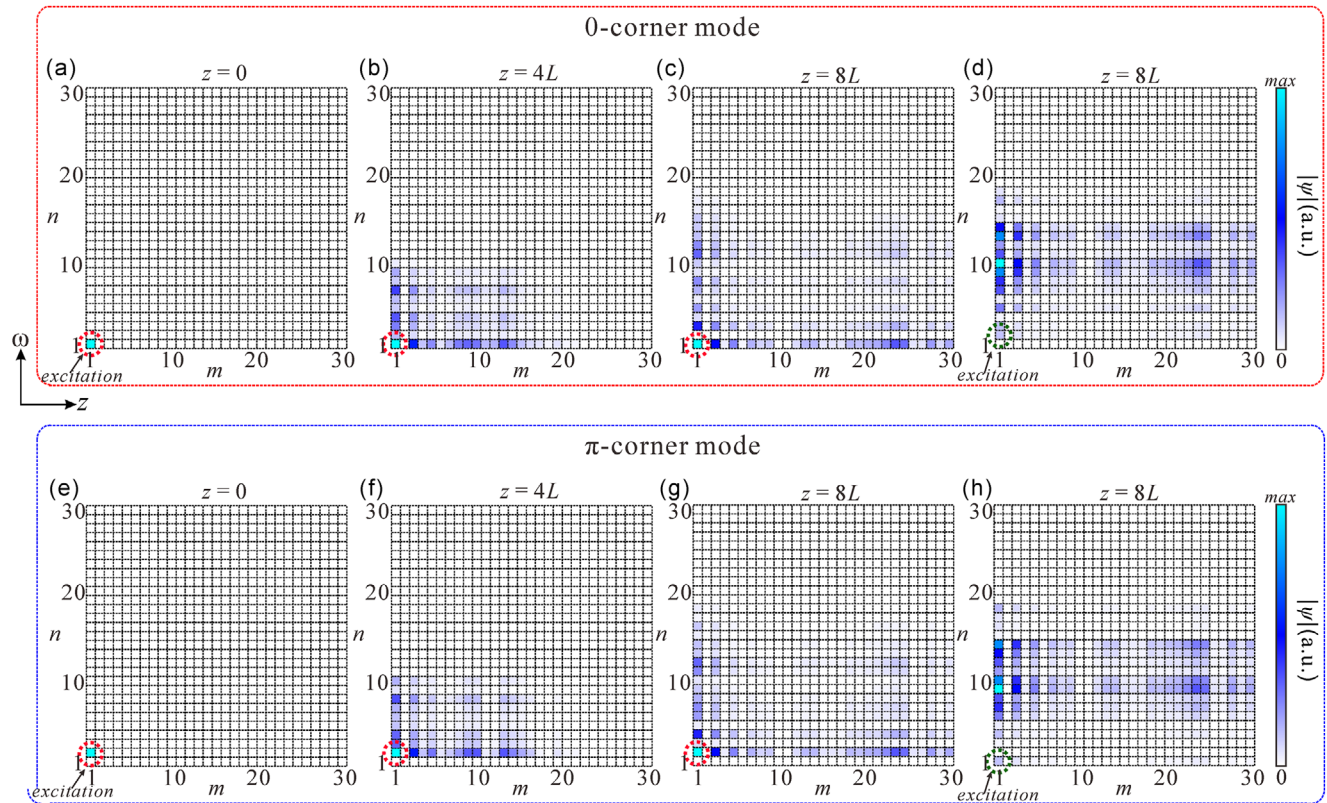


**Figure 4.** a–c) State distributions of the synthetic lattice at  $z = 0, 4L,$  and  $8L$  with coupling strength  $J_{s1} = 0.5\pi / L, J_{s2} = \pi / L$  and  $J_a = 0.5\pi / L, J_b = \pi / L$ , which supports the 0 corner states. The excited site locates at  $m = 1, n = 1$ , corresponding to the excitation at the first waveguide with frequency  $\omega = \omega_0 + \Omega_1$  and TE polarization. The red circle marks the excited corner state. d) State distributions of the synthetic lattice at  $z = 8L$  while the excited site is changed to  $m = 1, n = 2$ , which corresponds to the excitation with  $\omega = \omega_0 + \Omega_1 + \Omega_2$  and TM polarization. e–g) State distributions of the synthetic lattice at  $z = 0, 4L,$  and  $8L$  with coupling strength  $J_{s1} = 0.5\pi / L, J_{s2} = \pi / L$  and  $J_a = 1.5\pi / L, J_b = \pi / L$ , which supports the  $\pi$  corner states. The excited site locates at  $m = 1, n = 2$ , corresponding to the excitation at the first waveguide with frequency  $\omega = \omega_0 + \Omega_1 + \Omega_2$  and TM polarization. The red circle marks the excited corner state. h) State distributions of the synthetic lattice at  $z = 8L$  while the excited site is changed to  $m = 1, n = 1$ , which corresponds to the excitation with  $\omega = \omega_0 + \Omega_1$  and TE polarization.

applied along the crystal X axis. Such configuration would induce an off-diagonal perturbation to the relative permittivity as given by Equation (2), which leads to the transition between the TE and TM modes. In particular, for the LiNbO<sub>3</sub> waveguide, the electro-optical tensor element  $r_{51}$  is comparable with  $r_{33}$  which is often used in conventional traveling-wave modulators. Therefore, the modulation efficiency is compatible with that of conventional modulators in principle. Besides, when the 1D waveguide array is coupled together to realize the Floquet higher-order topological insulator, the microwave signals in adjacent electrodes would produce undesired crosstalk with each other. In our model, one could insert additional auxiliary waveguides in the waveguide array, so that the crosstalk between electrodes could be suppressed dramatically (see Section S5, Supporting Information).

### 3. Conclusion

In summary, we have proposed a scheme for realizing polarization-locked FHOTIs in synthetic frequency dimension through polarization inter-band transitions. Polarization degrees of freedom are introduced into the synthetic frequency lattice through photonic inter-band transitions. On this basis, by intro-

ducing Floquet periodic driving, 1D FTIs are created, and the related FHOTIs are further demonstrated by stacking the chains of the 1D Floquet topological insulators with dimerized couplings. In particular, the topological 0 and  $\pi$  mode of the FTIs occupy the frequency lattice with orthogonal polarization, which indicates polarization-locked topological states and enables selective excitation of the topological edge/corner states with specific polarizations. The introduction of inter-band transition in synthetic frequency lattice will provide more degrees of freedom for manipulating the light evolution, which can be extended to the researches containing pseudo-spin and non-Abelian gauge potentials. Our work lays the foundation for realizing controllable Floquet systems and opens an avenue for exploring higher-order topological physics with synthetic dimension, which shows great promise for applications in polarization conversion and quantum information processing.

### Supporting Information

Supporting Information is available from the Wiley Online Library or from the author.

## Acknowledgements

This work was supported by the National Natural Science Foundation of China (Grants No.62375097, No.12374305, No.11974124, No.12021004), and the Natural Science Foundation of Hubei Province (No.2023AFB822).

## Conflict of Interest

The authors declare no conflict of interest.

## Data Availability Statement

The data that support the findings of this study are available from the corresponding author upon reasonable request.

## Keywords

Floquet engineering, higher-order topology, photonic inter-band transitions, polarization-locked topological states, synthetic dimension

Received: July 24, 2024  
Revised: December 31, 2024  
Published online:

- [1] M. Li, D. Zhirihin, M. Gorchach, X. Ni, D. Filonov, A. Slobozhanyuk, A. Alù, A. B. Khanikaev, *Nat. Photon.* **2019**, *14*, 89.
- [2] M. S. Kirsch, Y. Zhang, M. Kremer, L. J. Maczewsky, S. K. Ivanov, Y. V. Kartashov, L. Torner, D. Bauer, A. Szameit, M. Heinrich, *Nat. Phys.* **2021**, *17*, 995.
- [3] B. Xie, H.-X. Wang, X. Zhang, P. Zhan, J.-H. Jiang, M. Lu, Y. Chen, *Nat. Rev. Phys.* **2021**, *3*, 520.
- [4] S. Chen, S. Ke, D. Zhao, J. Ye, Y. Wang, W. Liu, K. Huang, B. Wang, P. Lu, *Nano Lett.* **2024**, *24*, 4810.
- [5] W. A. Benalcazar, B. A. Bernevig, T. L. Hughes, *Science* **2017**, *357*, 61.
- [6] S. Franca, J. van den Brink, I. C. Fulga, *Phys. Rev. B* **2018**, *98*, 201114.
- [7] A. K. Ghosh, T. Nag, A. Saha, *Phys. Rev. B* **2021**, *103*, 045424.
- [8] A. K. Ghosh, G. C. Paul, A. Saha, *Phys. Rev. B* **2020**, *101*, 235400.
- [9] M. Rodriguez-Vega, A. Kumar, B. Seradjeh, *Phys. Rev. B* **2019**, *100*, 085138.
- [10] R. Seshadri, A. Dutta, D. Sen, *Phys. Rev. B* **2019**, *100*, 115403.
- [11] W. Zhu, Y. D. Chong, J. Gong, *Phys. Rev. B* **2021**, *103*, L041402.
- [12] H. Hu, B. Huang, E. Zhao, W. V. Liu, *Phys. Rev. Lett.* **2020**, *124*, 057001.
- [13] B. Huang, W. V. Liu, *Phys. Rev. Lett.* **2020**, *124*, 216601.
- [14] Y. Peng, G. Refael, *Phys. Rev. Lett.* **2019**, *123*, 016806.
- [15] T. Nag, V. Juričić, B. Roy, *Phys. Rev. Res.* **2019**, *1*, 032045.
- [16] W. Zhu, H. Xue, J. Gong, Y. Chong, B. Zhang, *Nat. Commun.* **2022**, *13*, 11.
- [17] N. Han, X. Xi, Y. Meng, H. Chen, Z. Gao, Y. Yang, *APL Photonics* **2024**, *9*, 010902.
- [18] M. Ehrhardt, S. Weidemann, L. J. Maczewsky, M. Heinrich, A. Szameit, *Laser Photonics Rev.* **2023**, *17*, 2200518.
- [19] D. Cheng, E. Lustig, K. Wang, S. Fan, *Light Sci. Appl.* **2023**, *12*, 158.
- [20] G. Li, L. Wang, R. Ye, Y. Zheng, D.-W. Wang, X.-J. Liu, A. Dutt, L. Yuan, X. Chen, *Light Sci. Appl.* **2023**, *12*, 81.
- [21] D. Yu, B. Peng, X. Chen, X.-J. Liu, L. Yuan, *Light Sci. Appl.* **2021**, *10*, 209.
- [22] S. Buddhiraju, A. Dutt, M. Minkov, I. A. D. Williamson, S. Fan, *Nat. Commun.* **2021**, *12*, 2401.
- [23] T. Chen, C. Huang, I. Velkovsky, K. R. A. Hazzard, J. P. Covey, B. Gadway, *Nat. Commun.* **2024**, *15*, 2675.
- [24] A. Dutt, L. Yuan, K. Y. Yang, K. Wang, S. Buddhiraju, J. Vučković, S. Fan, *Nat. Commun.* **2022**, *13*, 3377.
- [25] H. Zhao, B. Li, H. Li, M. Li, *Nat. Commun.* **2022**, *13*, 5426.
- [26] N. Englebort, N. Goldman, M. Erkintalo, N. Mostaan, S.-P. Gorza, F. Leo, J. Fatome, *Nat. Phys.* **2023**, *19*, 1014.
- [27] A. Senanian, L. G. Wright, P. F. Wade, H. K. Doyle, P. L. McMahon, *Nat. Phys.* **2023**, *19*, 1333.
- [28] S. K. Sridhar, S. Ghosh, D. Srinivasan, A. R. Miller, A. Dutt, *Nat. Phys.* **2024**, *20*, 843.
- [29] T. Ozawa, H. M. Price, *Nat. Rev. Phys.* **2019**, *1*, 349.
- [30] L. Yuan, Q. Lin, M. Xiao, S. Fan, *Optica* **2018**, *5*, 1396.
- [31] Z. Yan, S. Wan, Z. Wang, *Sci. Rep.* **2015**, *5*, 15927.
- [32] Q. Lin, M. Xiao, L. Yuan, S. Fan, *Nat. Commun.* **2016**, *7*, 13731.
- [33] A. Dutt, M. Minkov, Q. Lin, L. Yuan, D. A. B. Miller, S. Fan, *Nat. Commun.* **2019**, *10*, 3122.
- [34] A. Dutt, M. Minkov, I. A. D. Williamson, S. Fan, *Light Sci. Appl.* **2020**, *9*, 131.
- [35] K. Wang, B. A. Bell, A. S. Solntsev, D. N. Neshev, B. J. Eggleton, A. A. Sukhorukov, *Light Sci. Appl.* **2020**, *9*, 132.
- [36] K. Wang, A. Dutt, C. C. Wojcik, S. Fan, *Nature* **2021**, *598*, 59.
- [37] Y. Hu, M. Yu, N. Sinclair, D. Zhu, R. Cheng, C. Wang, M. Lončar, *Nat. Commun.* **2022**, *13*, 6293.
- [38] U. A. Javid, R. Lopez-Rios, J. Ling, A. Graf, J. Staffa, Q. Lin, *Nat. Photon.* **2023**, *17*, 883.
- [39] Y. Song, W. Liu, Z. Ling, Y. Zhang, B. Wang, P. Lu, *Phys. Rev. Appl.* **2020**, *14*, 064076.
- [40] X.-W. Luo, X. Zhou, C.-F. Li, J.-S. Xu, G.-C. Guo, Z.-W. Zhou, *Nat. Commun.* **2015**, *6*, 7704.
- [41] X.-W. Luo, X. Zhou, J.-S. Xu, C.-F. Li, G.-C. Guo, C. Zhang, Z.-W. Zhou, *Nat. Commun.* **2017**, *8*, 16097.
- [42] B. Y. Sun, X. W. Luo, M. Gong, G. C. Guo, Z. W. Zhou, *Phys. Rev. A* **2017**, *96*, 013857.
- [43] X.-F. Zhou, X.-W. Luo, S. Wang, G.-C. Guo, X. Zhou, H. Pu, Z.-W. Zhou, *Phys. Rev. Lett.* **2017**, *118*, 083603.
- [44] X.-W. Luo, C. Zhang, G.-C. Guo, Z.-W. Zhou, *Phys. Rev. A* **2018**, *97*, 043841.
- [45] L. Yuan, Q. Lin, A. Zhang, M. Xiao, X. Chen, S. Fan, *Phys. Rev. Lett.* **2019**, *122*, 083903.
- [46] M. Yang, H.-Q. Zhang, Y.-W. Liao, Z.-H. Liu, Z.-W. Zhou, X.-X. Zhou, J.-S. Xu, Y.-J. Han, C.-F. Li, G.-C. Guo, *Nat. Commun.* **2022**, *13*, 2040.
- [47] E. Lustig, S. Weimann, Y. Plotnik, Y. Lumer, M. A. Bandres, A. Szameit, M. Segev, *Nature* **2019**, *567*, 356.
- [48] E. Lustig, L. J. Maczewsky, J. Beck, T. Biesenenthal, M. Heinrich, Z. Yang, Y. Plotnik, A. Szameit, M. Segev, *Nature* **2022**, *609*, 931.
- [49] A. Regensburger, C. Bersch, M.-A. Miri, G. Onishchukov, D. N. Christodoulides, U. Peschel, *Nature* **2012**, *488*, 167.
- [50] S. Weidemann, M. Kremer, S. Longhi, A. Szameit, *Nat. Photon.* **2021**, *15*, 576.
- [51] S. Wang, C. Qin, W. Liu, B. Wang, F. Zhou, H. Ye, L. Zhao, J. Dong, X. Zhang, S. Longhi, P. Lu, *Nat. Commun.* **2022**, *13*, 7653.
- [52] Y. Guan, J. Zhang, L. Li, R. Cao, G. Wang, J. Chen, X. Wang, B.-O. Guan, J. Yao, *Commun. Phys.* **2023**, *6*, 258.
- [53] L. Yuan, Y. Shi, S. Fan, *Opt. Lett.* **2016**, *41*, 741.
- [54] A. Dutt, Q. Lin, L. Yuan, M. Minkov, M. Xiao, S. Fan, *Science* **2020**, *367*, 59.
- [55] Q. Lin, X.-Q. Sun, M. Xiao, S.-C. Zhang, S. Fan, *Sci. Adv.* **2018**, *4*, eaat2774.
- [56] J. Suh, G. Kim, H. Park, S. Fan, N. Park, S. Yu, *Phys. Rev. Lett.* **2024**, *132*, 033803.
- [57] C. Qin, L. Yuan, B. Wang, S. Fan, P. Lu, *Phys. Rev. A* **2018**, *97*, 063838.

- [58] C. Qin, F. Zhou, Y. Peng, D. Sounas, X. Zhu, B. Wang, J. Dong, X. Zhang, A. Alù, P. Lu, *Phys. Rev. Lett.* **2018**, *120*, 133901.
- [59] M. Fruchart, *Phys. Rev. B* **2016**, *93*, 115429.
- [60] Q. Cheng, Y. Pan, H. Wang, C. Zhang, D. Yu, A. Gover, H. Zhang, T. Li, L. Zhou, S. Zhu, *Phys. Rev. Lett.* **2019**, *122*, 173901.
- [61] Z. Yu, S. Fan, *Nat. Photon.* **2009**, *3*, 91.
- [62] J. Wang, Y. Shi, S. Fan, *Opt. Express* **2020**, *28*, 11974.
- [63] K. Fang, Z. Yu, S. Fan, *Phys. Rev. Lett.* **2012**, *108*, 153901.
- [64] H. Lira, Z. Yu, S. Fan, M. Lipson, *Phys. Rev. Lett.* **2012**, *109*, 033901.
- [65] R. W. Bomantara, L. Zhou, J. Pan, J. Gong, *Phys. Rev. B* **2019**, *99*, 045441.